A new fusion algorithm for shadow penetration using visible and midwave infrared polarimetric images

Daniel A. Lavigne
Defence Research and Development Canada
Quebec, Canada
daniel.lavigne@drdc-rddc.gc.ca

Melanie Breton
Aerex Avionics Inc.
Breakeyville (Qc), Canada
melanie.breton.aerex@drdc-rddc.gc.ca

Abstract – *This paper presents a new polarimetric image fusion algorithm to discriminate objects lying in shadow areas against cluttered backgrounds. Polarimetric signatures of man-made objects are collected using a fully automated passive polarimetric sensor-suite operating in the visible, shortwave, midwave, and longwave infrared bands. The polarization state of the radiation emitted and/or reflected from objects' surfaces and surrounding background is characterized using the total intensity, the degree of linear polarization, and the phase of the polarization. Using two distinct scenarios, experimental results demonstrate the utility of the proposed image fusion algorithm to exploit the polarized signatures of man-made objects in the visible and midwave infrared bands for shadow penetration purposes.*

Keywords: Polarimetric images, shadow penetration, image fusion algorithm, target enhancement.

1 Introduction

Spectral sensors are commonly used to measure the intensity of optical radiation and to provide spectral information about the distribution of material components in a given scene, over a limited number of wave bands. Information provided by such sensors can be used for applications ranging from target detection and recognition to feature mapping and extraction of geographic information systems (GIS).

The electro-magnetic radiation emitted and reflected from a smooth surface observed near a grazing angle becomes partially polarized in the visible and infrared wavelength bands [1] [2]. Accordingly, infrared polarization contrast still exists even when the temperature difference between the target and its background is negligible [3]. Considering this, it is meaningful to investigate the polarization of light as an additional way of extracting information about the shape, shading, roughness, and surface features of targets of interest in cluttered backgrounds. The overall performance of target detection algorithms could be increased by exploiting these polarimetric signatures to discriminate man-made objects located in shadow areas [4]. This can be achieved through the use of metrics, derived from the computed Stokes parameters, to define the degree of polarization of man-made objects. To this end, this paper exploits the polarization signatures of man-made objects acquired by a fully automated passive polarimetric imaging sensor-suite developed at DRDC Valcartier [5]. Within a polarimetric imaging fusion framework operating in the visible and midwave infrared bands, acquired target signatures are processed using an advanced fusion algorithm to perform shadow penetration. A metallic aluminum plate and a Sport Utility Vehicle (SUV) are used as targets of interest, both located to generate shadow areas within the scene. In order to appreciate the efficiency of the proposed image fusion algorithm, its performance is compared to a recent one developed by Zhao *et al.* [6]. Experimental results using these two different scenarios confirmed the effectiveness of the proposed image fusion algorithm for shadow penetration purposes using polarized light in the visible and midwave infrared bands.

The paper is organized as follows. Section 2 describes the polarimetric sensor-suite used to collect polarized signatures of man-made objects. Section 3 presents the backgrounds related to the use of polarized light within a fusion framework for target detection and shadow penetration purposes. Section 4 illustrates results of experimental measurements by means of the methodology developed and its application on two different case scenarios. Finally, section 5 concludes the paper and suggests ways to improve further the proposed image fusion algorithm.

2 Polarimetric imaging sensor-suite

This section presents the hardware setup and the data acquisition process of the VIP SPICE^{TM}system, used to collect polarization signatures of targets of interest.

2.1 Hardware system

The *Visible Infrared Passive Spectral Polarimetric Imager for Contrast Enhancement* (VIP SPICE^{TM}) operates a suite of four sensors concomitantly in the visible (VIS), the shortwave infrared (SWIR), the midwave infrared (MWIR), and

the longwave infrared (LWIR) bands. Additionally, a seven-position filter wheel containing six different filters (400 nm, 436 nm, 490 nm, 530 nm, 550 nm, 690 nm) is mounted in front of the visible sensor. The sensor-suite is made of four synchronously-rotating polarizers mounted in front of each of the four individual sensors. A single belt links all the polarizers so their rotation is synchronized. This setup enables the acquisition of a scene at different polarization angles. Linear polarizers are oriented successively at 0, 45, 90, and 135 degrees and along specific time intervals. The four-sensor suite is mounted on a motorized pan & tilt platform device. The calibration, data acquisition, and data processing are fully automated. The computer controls the entire capture process: from aligning the pan & tilt toward the target to the data acquisition. The capture process includes the calibration, the capture and the display of the images. The cameras are plugged individually to an input frame grabber card (DFG/MC4). For every capture, five images are acquired at each polarization angle by all sensors. Then, the polarizers are flipped up and five unpolarized images are acquired. The entire capture process takes less than 2m30s to perform. Precise geolocation of the sensor and the targets are achieved using a GPS receiver and a range finder, respectively. A 30 degrees visible camera provides a global view of the scene. Acquired data are remotely accessible and process on a standalone workstation. Figure 1 illustrates the setup of the VIP SPICE^{TM}sensor.

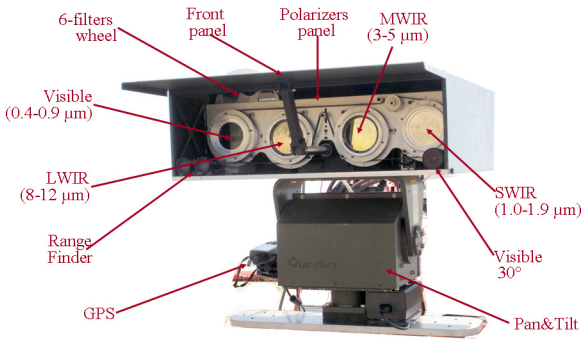

Figure 1: Setup of the VIP SPICE^{TM}sensor. The sensor operates a suite of four cameras concomitantly in the visible (VIS), the shortwave infrared (SWIR), the midwave infrared (MWIR), and the longwave infrared (LWIR) bands

The VIP SPICE's visible sensor is a CCD camera imager (LM165 from Lumenera) that operates in the 400 to 900 nm. The camera has 1392 x 1040 pixels resolution and a field of view (FOV) of 5 degrees. The polarizer used is a linear polarizer from Edmund Optics. The shortwave infrared camera is a solid-state InGaAs imager (SU320MSW-1.7RT from Sensors Unlimited) that operates in the 0.9 to 1.7 μm. The camera has 320 x 256 pixels with a FOV of 20 degrees. The SWIR band uses aluminum microwires on a glass substrate as a polarizer from Versalight. The midwave infrared camera is an IR-M700 from Mitsubishi. It is a focal plane array (platinum silicide) that operates from 1.2 to 5.9 μm. It has a focal plane array of 801 x 512 pixels with a FOV of 12 degrees. The polarizer used is a wire-grid ZnSe from Medway Optics. The longwave infrared camera used is an uncooled microbolometer E6000 Thermal Imager from Nytech that operates in the 8 to 12 μm spectral range and has a 640 x 480 pixels array infrared module, with a FOV of 10 degrees. The gain and the offset can be set to a manual mode. The Non-Uniformity Correction (NUC) is done by closing the front panel before the acquisition. The field of view is around $10°$x$10°$. The polarizer used is a wire-grid ZnSe from Reflex Analytical Corp. positioned directly in front of the lens. Figure 2 shows a close-up view of the VIP SPICE^{TM}sensor.

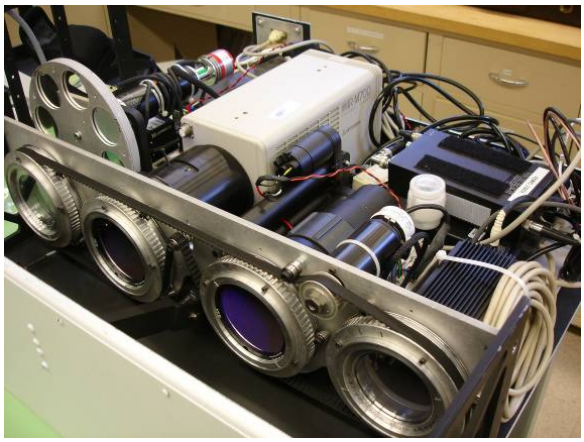

Figure 2: Close-up view of the VIP SPICE^{TM}sensor.

3 Target detection and shadow penetration using polarized light

While the light originating from the sun is not polarized, polarization is an intrinsic property of light that can be used for target detection [7]. Indeed, most of the light reflected or scattered from object surfaces is partially polarized [6]. Accordingly, polarization parameters can be estimated and used to characterize the polarization state of the radiation emitted and reflected by such target surfaces [8]. Next subsections describe a fusion framework, where Stokes parameters of some targets, acquired in the visible and midwave infrared bands by the VIP SPICE^{TM}sensor, are used to accentuate the detection of man-made objects located in shadow areas.

3.1 Stokes vector

Polarized electromagnetic radiation is the resultant of the interaction of the ensemble waves propagated in the same direction but with different phase and amplitude. The representation of the radiation backscattered by the targets - partially, completely, circularly or elliptically polarized - is

achieved through the use of the Stokes vector:

$$\mathbf{F} = \begin{bmatrix} \mathbf{I} \\ Q \\ U \\ V \end{bmatrix} = \begin{bmatrix} I \\ I\cos 2\psi \cos 2\chi \\ I \sin 2\psi \cos 2\chi \\ I \sin 2\chi \end{bmatrix} = \begin{bmatrix} < A_x^2 + A_y^2 > \\ < A_x^2 - A_y^2 > \\ 2A_xA_y \cos\gamma \\ 2A_xA_y \sin\gamma \end{bmatrix} = \begin{bmatrix} S_0 \\ S_1 \\ S_2 \\ S_3 \end{bmatrix} \quad (1)$$

where I is the intensity of radiation whose geometrical parameters (ellipticity angle χ and ellipse orientation angle ψ characterize the electromagnetic wave polarization. A_x, A_y are the amplitudes of the electromagnetic waves in mutually perpendicular directions, A^2 is the intensity, γ is the phase angle between A_x and A_y, and $<>$ indicates time averaging. The Stokes parameters are all related by $I^2 = Q^2+U^2+V^2$, so only three of them are independent. Q is the difference in radiant intensity between the orthogonal x and y directions used to specify A_x and A_y. I and Q can be obtained by passing light waves through linear polarizers at 0 and 90 degrees respectively, while U indicates the excess of radiation in the $+45^\circ$ direction over that in the $+135^\circ$ direction relative to the plane of vision. V is the circularly polarized component in the radiation. Figure 3 illustrates the polarization of the electromagnetic waves, where the electric $\vec{E}$ and magnetic $\vec{H}$ fields are orthogonally propagating along the energy propagation direction $\vec{k}$, forming a polarization ellipse by the projection of the electrical field trajectory in the transverse plan. Linear polarization states (i.e. S_1 and S_2) are formed when $\chi = 0$. The amount of circular polarized radiation, V, is produced when $\chi = 1$.

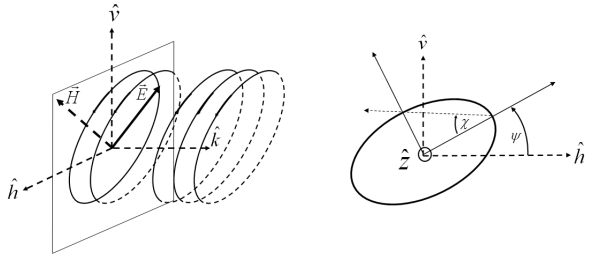

(a) (b)

Figure 3: The polarization of electromagnetic waves. 3(a) The magnetic $\vec{H}$ and electric $\vec{E}$ fields are positioned in orthogonal directions and contained within the transverse plan of the electromagnetic wave along the energy propagation direction $\vec{k}$. 3(b) Polarization ellipse formed by the projection of the electrical field trajectory in the transverse plan during its propagation.

Consequently, S_0 represents the total intensity of the signal, while S_1 is the portion of incident radiation polarized either parallel to or perpendicular to the axis defined by $\psi = 0$, and S_2 describes light polarized along axes $\psi = 45$ and $\psi = 135$ degrees. Using these Stokes parameters, additional metrics can be computed to describe further the behaviour of polarized light and yield additional information about the roughness and material of the target surface.

3.2 Polarization parameters

The difference in the way light reflects from different kinds of materials can be expressed by the polarization state of the targets surfaces. Indeed, using the Stokes vector (eq. 1), additional parameters can be computed to reflect the object surface characteristics for target discrimination purposes [9]. For instance, the ratios of the reflected wave amplitude to the incident wave amplitude for incident light that is linearly polarized parallel/perpendicularly to the plane of specular incidence can be computed using the Fresnel equations [10]. These ratios depend upon the angle of incidence and the refraction index of the reflecting material. Consequently, the Fresnel equations can be used to compute all incident polarization states of a given material. Moreover, considering that the refraction index of a material is a function of the wavelength, the intensity of the reflected light from the target surfaces (which is either specular or diffuse) will fluctuate with the variation of the wavelength [6].

While the measured intensity of light is composed of two parts, the polarized light can be described by three single elements: the total intensity, the degree of polarization, and the phase of the polarization.

For unpolarized diffuse component, the total intensity S_0 is defined as:

$$S_0(\eta, \lambda, \theta_i) = \alpha_{min}(\eta, \lambda, \theta_i) + \alpha_{max}(\eta, \lambda, \theta_i) \quad (2)$$

where α_{min} and α_{max} are two parameters defined by:

$$\alpha_{min}(\eta, \lambda, \theta_i) = \frac{1}{2}\alpha_d + \frac{\tau_\parallel^2(\eta, \lambda, \theta_i)}{\tau_\parallel^2(\eta, \lambda, \theta_i) + \tau_\perp^2(\eta, \lambda, \theta_i)}\alpha_s \quad (3)$$

$$\alpha_{max}(\eta, \lambda, \theta_i) = \frac{1}{2}\alpha_d + \frac{\tau_\perp^2(\eta, \lambda, \theta_i)}{\tau_\parallel^2(\eta, \lambda, \theta_i) + \tau_\perp^2(\eta, \lambda, \theta_i)}\alpha_s \quad (4)$$

and where η is the refraction index of the object surface material, and θ_i is the angle of incidence. $\tau_\parallel$ et $\tau_\perp$ are the amplitude reflection coefficients for light polarized parallel and perpendicular to the plane of incidence, respectively, and are defined by:

$$\begin{aligned} \tau_\parallel(\eta_i, \eta, \theta_i, \theta_r) &= \frac{\xi_{r\parallel}(\eta_i, \eta, \theta_i, \theta_r)}{\xi_{i\parallel}} \\ &= \frac{\eta\cos\theta_i - \eta_i\cos\theta_r}{\eta\cos\theta_i + \eta_i\cos\theta_r} \end{aligned} \quad (5)$$

$$\begin{aligned} \tau_\perp(\eta_i, \eta, \theta_i, \theta_r) &= \frac{\xi_{r\perp}(\eta_i, \eta, \theta_i, \theta_r)}{\xi_{i\perp}} \\ &= \frac{\eta_i\cos\theta_i - \eta\cos\theta_r}{\eta_i\cos\theta_i + \eta\cos\theta_r} \end{aligned} \quad (6)$$

where θ_r is the angle of refraction, $\xi_{i\|}$and $\xi_{r\|}$ are the incident and refracted polarization components parallel to the specular plane, and $\xi_{r\perp}$ and $\xi_{i\perp}$ are the incident and refracted polarization components perpendicular to the specular plane, respectively.
Spectral reflectance is the ratio of the energy reflected from a surface in a given waveband to the energy incident in that waveband, which depends on the material composition. It reflects the variation of ratios of energy at different wavelengths, while polarization reflects the variation of ratios or energy at different vibration directions. The spectral reflectance at wavelength λ is defined as:

$$\tau(\lambda, \eta_i, \eta, \theta_i, \theta_r) = \frac{\xi_r(\lambda, \eta_i, \eta, \theta_i, \theta_r)}{\xi_i(\lambda)} \tag{7}$$

Subsequently, the degree of linear polarization (DoLP) derived from the degree of polarization, can be calculated using the linear information and normalizing it for the intensity, such as:

$$DoLP(\eta, \lambda, \theta_i) = \frac{\tau_\perp^2(\eta, \lambda, \theta_i) - \tau_\|^2(\eta, \lambda, \theta_i)}{\tau_\perp^2(\eta, \lambda, \theta_i) + \tau_\|^2(\eta, \lambda, \theta_i)} \cdot \frac{1}{1+\zeta} \tag{8}$$

where $\zeta = \frac{\alpha_d}{\alpha_s}$ is the ratio between the diffuse and specular components of reflection.
The phase of polarization, which is the orientation of the major axis of the polarization ellipse, represents the polarizer angle where the intensity be the strongest. It is computed by:

$$\phi = \frac{1}{2} \arctan\Big(\cos(\beta) \cdot \tan(2\chi)\Big) \tag{9}$$

where $\tan\chi = \frac{A_y}{A_x}$, β is the relative phase shift, and A_x, A_y are the maximum amplitudes in the x, y directions.

3.3 Fusion of polarimetric images

In this paper, we propose to detect targets from their background using the polarimetric and spectral characteristics of specular and diffuse reflected light acquired from the targets. Processing the total intensity (S_0), the DoLP and the polarization angle (ϕ), a false color rendering of the scene is generated [11]. Building on recent work [6], the fusion process can be summarized as follows:

1. Image preprocessing, including normalization and denoising using state-of-the-art linear filters [12].

2. Image co-registration [13] is performed with computation of mutual information $MI(u, v)$, as defined by [14]:

$$MI(u,v) = \sum_f \sum_g \rho_{FG}(f, g|u, v) \cdot \log\left(\frac{\rho_{FG}(f, g|u, v)}{\rho_F(f)\rho_G(g)}\right) \tag{10}$$

where f and g are allowed intensity values in the template image G and window image F. $\rho_G(g)$ and $\rho_F(f)$ are the probability mass functions of the intensity values in G and F. $\rho_{FG}(f, g|u, v)$ is the joint probability mass functions of the images given the relative shift (u, v) between them.

3. The common component (CC), implemented as a local minimum operator of the three polarized images, is found in each polarized image [6]:

$$CC = S_0 \cap DoLP \cap \phi \tag{11}$$

and is then defined by:

$$CC = \min\{\min\{\phi, DoLP\}, S_0\} \tag{12}$$

4. The unique contribution of each image can be calculated using the common component information:

$$\begin{aligned} S_0^* &= S_0 - (S_0 \cap DoLP \cap \phi) && (13)\\ DoLP^* &= DoLP - (S_0 \cap DoLP \cap \phi) && (14)\\ \phi^* &= \phi - (S_0 \cap DoLP \cap \phi) && (15) \end{aligned}$$

5. Image adjustment is then performed:

$$\begin{aligned} S_0^{**} &= S_0 - DoLP^* - \phi^* && (16)\\ DoLP^{**} &= DoLP - {S_0}^* - \phi^* && (17)\\ \phi^{**} &= \phi - DoLP^* - S_0^* && (18) \end{aligned}$$

6. Fusing the images following the conversion HSV to RGB color maps [11] and renormalizing yields:

$$\sum = HSV\{S_0^{**}, DoLP^{**}, \phi^{**}\} \tag{19}$$

7. Post-processing of the resultant fused images is performed using edge detection algorithms [12].

In order to improve the contrast enhancement performance of the polarimetric fusion algorithm for shadow penetration purposes [15], the phase orientation information (eq. 11) is replaced by the following measure of polarization [16] :

$$\nabla = 2\frac{(I_0^\kappa - I_{90}^\kappa + 16)^{\frac{1}{\kappa}} + (I_{45}^\kappa - I_{135}^\kappa + 16)^{\frac{1}{\kappa}}}{(I_0^\kappa + I_{90}^\kappa + I_{45}^\kappa + I_{135}^\kappa)} \tag{20}$$

where κ is a constant equal to 0.25 and I_0, I_{45}, I_{90}, I_{135} are the orientation in degrees of the polarizer in front of the sensors.

Replacing equation 20 in equations 11- 19 yields:

$$CC = S_0 \cap DoLP^* - \nabla \tag{21}$$

and then the following equations for the image adjusment:

$$\begin{aligned} S_0^{**} &= S_0 - DoLP^* - \nabla^* && (22)\\ DoLP^{**} &= DoLP - S_0^* - \nabla^* && (23)\\ \nabla^{**} &= \nabla - DoLP^* - S_0^* && (24) \end{aligned}$$

4 Experimental measurements

In order to test the performance of the new proposed shadow penetration algorithm, polarimetric signatures of man-made objects were collected using DRDC Valcartier's VIP SPICE^{TM}sensor during field experiments conducted in Summer time [5].

Two distinct man-made objects have been used to test the performance of the algorithm: a metallic aluminum plate with tapes and a standard SUV. Both objects where placed within the scene in order to generate shadow areas covering a portion of the objects. Figure 4 illustrates the two man-made objects used as targets of interest.

(a) (b)

Figure 4: Man-made objects used as targets of interest. 4(a) Metallic aluminum plate with tapes. 4(b) A standard Sport Utility Vehicle (SUV).

Experimental results demonstrate the utility of the proposed fusion algorithm to use the polarization signatures of man-made objects in the visible and midwave infrared bands for shadow penetration purposes.

Figure 5 illustrates computed results for the metallic aluminum plates with tapes, in the visible band. The polarimetric fusion algorithm successfully detected the whole metallic plate from the natural background, even in the shadow area (5(d), left portion of the plate). The performance of the algorithm is greater than the one generated using the algorithm implemented in [6] (5(c)).

Figure 6 shows computed results for the SUV scenario in the MWIR band. The SUV's tires in shadow area are fully detected by the shadow penetration algorithm (6(d)), providing detection results superior than previous algorithm [6] (6(c)). Thus, this shadow penetration performance is provided at the cost of losing some details about the hood and the roof rack of the SUV.

Figure 7 illustrates the final computed results of the polarimetric fusion algorithm, followed by a post-processing step including the detection of edges. The outlines of the metallic plate are detected as a whole, including the portion in shadow area (7(a)). The SUV's tires are easily discernible, even the area below the vehicle (7(b)).

5 Conclusion

A new polarimetric image fusion algorithm designed to discriminate man-made objects in shadow areas has been presented. Polarimetric signatures of different targets of interest were collected by means of a fully automated passive polarimetric sensor-suite operating simultaneously in the VIS/SWIR/MWIR/LWIR bands. The sensor-suite is made of four synchronously-rotating polarizers mounted in front of each of the four individual sensors, linked together by a single belt.

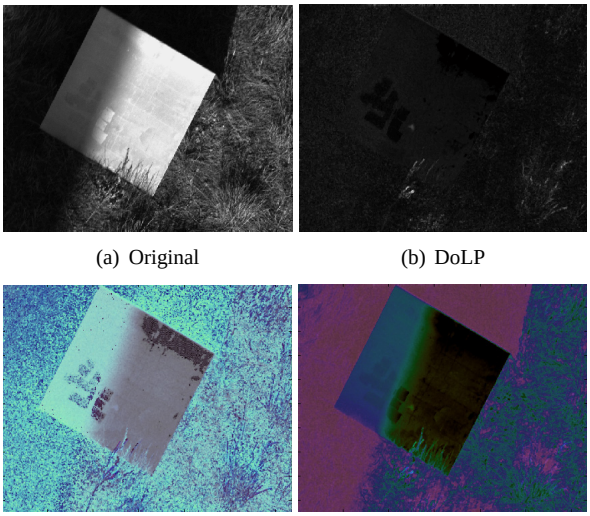

(a) Original (b) DoLP

(c) Zhao's algorithm (d) Shadow penetration

Figure 5: Fusion results for a metallic aluminum plate in the Visible band. 5(a) Original image where a portion is in shadow. 5(b) Computed degree of linear polarisation (DoLP). 5(c) Zhao's algorithm implemented in [6] and 5(d) results from the proposed shadow penetration algorithm (showed in pseudo color maps).

Using the polarized light information gathered from the objects surface characteristics, the total intensity, the degree of linear polarization, and the phase of the polarization have been computed by means of the Stokes vector. Experimental measurements demonstrated that it is possible to exploit the polarimetric response of man-made objects for target detection purposes.

Moreover, the new polarimetric image fusion algorithm was evaluated for its capability to perform shadow penetration in two different case scenarios. Experimental results demonstrated the utility of such shadow penetration algorithm on polarimetric images acquired in the visible and midwave infrared bands. Furthermore, the performance of the algorithm on the two case scenarios was greater than previous algorithm.

Future work will integrate the other infrared bands of the sensor-suite (i.e. shortwave and longwave infrared bands) into the fusion process as an attempt to improve further the target detection capability of the shadow penetration algorithm. Building on the results achieved, it is expected that such fusion scheme will provide a superior detection capability of difficult targets, embedded in shadowed areas and cluttered backgrounds.

(a) Original (b) DoLP

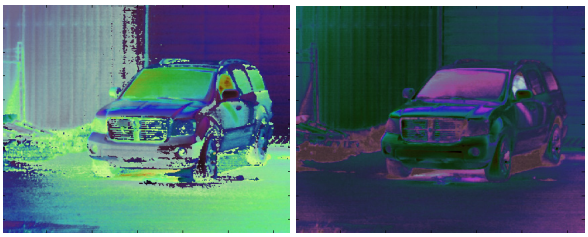

(c) Zhao's algorithm (d) Shadow penetration

Figure 6: Fusion results for the SUV in the MWIR band. 6(a) Original image. 6(b) Degree of linear polarisation (DoLP). Contrast enhancement using 6(c) Zhao's algorithm implemented in [6] and 6(d) results from the proposed shadow penetration algorithm (showed in pseudo color maps).

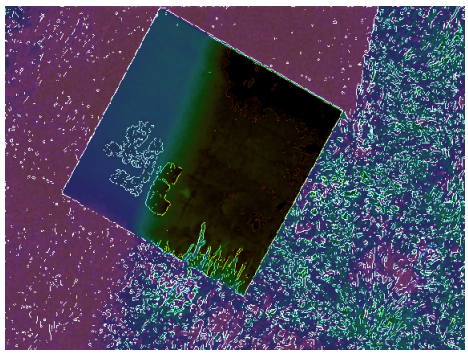

(a)

(b)

Figure 7: Edge detection as postprocessing step. 7(a) Outlines of the plate are highlighted. 7(b) Outlines of the tires are discernible in shadow areas.

References

[1] S.-S. Lin, K.M. Yemelyanov, E.N. Pugh, Jr., and N. Engheta, "Separation and contrast enhancement of overlapping cast shadow components using polarization," *Optics Express*, Vol. 14, No. 16, 7 August 2006, pp. 7099–7108.

[2] F. Cremer, P.B.W. Schwering, W. de Jong, K. Schutte, and A.N. de Jong, "Infrared polarization measurements of targets and backgrounds in a marine environment," *Proc. SPIE Vol. 4370*, Targets and Backgrounds VII: Characterization and Representation, Orlando (FL), 16-20 April 2001, pp. 169–180.

[3] D.A. Lavigne, M. Breton, G. Fournier, M. Pichette, and V. Rivet, "A new passive polarimetric imaging system collecting polarization signatures in the visible and infrared bands," *Proc. SPIE Vol. 7300*, Infrared Imaging Systems: Design, Analysis, Modeling, and Testing XX, Orlando (FL), 13-17 April 2009, pp. 1–10.

[4] M.J. Duggin, and M.L. Pugh, "Data fusion: a consideration of metrics and the implications for polarimetric imagery," *Proc. SPIE Vol. 5888*, Polarization Science and Remote Sensing II, San Diego (CA), 2-4 August 2005, pp. 304–314.

[5] D.A. Lavigne, M. Breton, M. Pichette, V. Larochelle, and J.-R. Simard, "Evaluation of active and passive polarimetric electro-optic imagery for civilian and military target discrimination," *Proc. SPIE Vol. 6972*, Polarization: Measurements, Analysis, and Remote Sensing VIII, Orlando (FL), 16-20 March 2008, pp. 1–9.

[6] Y. Zhao, L. Zhang, D. Zhang, and Q. Pan, "Object separation by polarimetric and spectral imagery fusion," *Computer Vision and Image Understanding*, Vol. 113, No. 8, August 2009, pp. 855–866.

[7] J.S. Tyo, M.P. Rowe, E.N. Pugh, Jr., and N. Engheta, "Target detection in optical scattering media by polarization-difference imaging," *Appl. Opt.*, Vol. 35, 1996, pp. 1855–1870.

[8] D.A. Lavigne, M. Breton, G. Fournier, M. Pichette, and V. Rivet, "Development of performance metrics to characterize the degree of polarization of man-made objects using passive polarimetric images," *Proc. SPIE Vol. 7336*, Signal Processing, Sensor Fusion, and Target Recognition XVIII, Orlando (FL), 13-17 April 2009.

[9] D.A. Lavigne, M. Breton, M. Pichette, V. Larochelle, and J.-R. Simard, "Enhanced military target discrimination using active and passive polarimetric imagery," *IEEE International Geoscience & Remote Sensing Symposium 2008*, Boston (MA), 6-11 July 2009.

[10] D. Goldstein, “Polarized light, 2nd edition,” Marcel Dekker, New York, 2003.

[11] A. Toet, and J. Walraven, “New false colour mapping for image fusion,” *Optical Engineering*, Vol. 35, No. 3, March 1996, pp. 650–658.

[12] R. Jain, R. Kasturi, and B.G. Schunck, “Machine Vision,” McGraw-Hill, 1995.

[13] D.A. Lavigne, “A fully automated image co-registration system,” *Proc. SPIE Vol. 6235*, Signal Processing, Sensor Fusion, and Target Recognition XV, Orlando (FL), 17-21 April 2006.

[14] D.A. LeMaster, “A comparison of template matching registration methods for polarimetric imagery,” *IEEE Aerospace Conference 2008*, Vol. 1, 1-8 March 2008, pp. 1–9.

[15] M.J. Duggin, and G.J. Kinn, “Vegetative target enhancement in natural scenes using multiband polarization methods,” *Proc. SPIE Vol. 4481*, Polarization Analysis, Measurement and Remote Sensing IV, San Diego (CA), 30 July - 1 August 1997, pp. 288–295.

[16] M.J. Duggin, G.J. Kinn, and E.H. Bohling, “Contrast enhancement using multiband polarization methods,” *Proc. SPIE Vol. 3121*, Polarization Analysis, Measurement and Remote Sensing IV, San Diego (CA), 30 July - 1 August 1997, pp. 288–295.